Proceedings of the 9th International Workshop on Ship and Marine Hydrodynamics, 26 – 28 August 2015, Glasgow, UK

Numerical Simulation of 3D Sloshing Flows in a Rectangular Tank by MPS Method

Yaqiang Yang[1,2], Zhenyuan Tang[1,2] and Decheng Wan[1,2*]

1. State Key Laboratory of Ocean Engineering, School of Naval Architecture, Ocean and Civil Engineering, Shanghai Jiao Tong University,
2. Collaborative Innovation Center for Advanced Ship and Deep-Sea Exploration, Shanghai 200240, China

Abstract: Liquid sloshing in a 3D rectangular tank under multiple degrees of freedom (DOF) excitations is simulated by the in house solver MLParticle-SJTU based on Moving Particle Semi-Implicit (MPS) method. Firstly, liquid sloshing under horizontal and angular motion is carried out to validate the present particle solver MLParticle-SJTU respectively. The comparison between the numerical flow pattern and impact pressure and the corresponding experimental data shows that MLParticle-SJTU is reliable and efficient to solve 3D sloshing problem. In addition, the present model is extended to 3D liquid sloshing with multiple degrees of freedom motions. The evolution of sloshing waves and impact pressure are analyzed to investigate the coupling effect of different DOF excitations. Results show that surge motion and rolling motion have weak interaction with each other. Sloshing can be damped if the amplitude and phase difference between surge motion and pitch motion are appropriate.

Keywords: MPS method; 3D liquid sloshing; flow pattern; impact pressure; multiple DOF excitations

1 Introduction

Sloshing refers to the movement of liquid inside a partially filled tank due to external excitations. Liquid sloshing is of significant importance in coastal and offshore engineering and marine industry. When the amplitude of the ship motion is very large or its frequency is close to the natural frequency of the liquid tank, violent sloshing flows may appear, exerting strong impact pressure on the wall of the tank, which may cause too large deformation on the structure locally, and further affect the stability of ship globally. Therefore, it's essential to predict the impact pressure accurately to avoid severe structural damage.

Due to the ever-increasing interests in liquid sloshing, a number of researchers have applied numerical simulation methods to the sloshing problem. Wu and Chen (2009) employed a finite difference method (FDM) solver to investigate sloshing waves in 3D liquid tank subjected to a range of excitation frequencies with motions that exhibit multiple degrees of freedom. Liu and Lin (2007) developed a 3D two phase model with second order VOF method and performed simulations with a broken free surface under six DOF excitations. Kim (2001) applied the SOLA-SURF method to simulate sloshing flows in 2D and 3D containers and adopted a buffer zone concept to calculate the impact pressure on the tank ceiling. Hu et al. (2004) employed an improved constraint interpolation profile (CIP) method to investigate violent sloshing flow in a horizontally oscillating rectangular tank.

Most of these simulations discussed above are based on grid-based methods. In recent years, meshfree methods such as SPH (Smoothed Particle Hydrodynamics, Gingold and Monaghan, 1977) and MPS (Moving Particle Semi-Implicit, Koshizuka and Oka, 1996; Koshizuka et al., 1998) have been developed to model fluid motion with large deformation of free surface. In particle method, flow is modeled as an assembly of interacting particles which have physical properties, such as mass, momentum, and energy, etc. Since these particles have no fix topography among each other, meshless methods are more flexible to deal with the large deformed free surface flows (Zhang and Wan, 2011a).

Until now, there has been some work on liquid sloshing based on particle method. Cui and Liu (2009) applied SPH to simulate the sloshing phenomenon in a 2D tank subject to the motion of surge and pitch，showing a good agreement between numerical simulation and experiment in terms of free surfaces deformation, but overestimated impact pressure. Shao et al (2012) implied SPH method to model viscous incompressible liquid sloshing with different external excitations and different structures. The obtained numerical results including flow pattern, wave height, pressure field, and pressure load on solid walls were agreeable with experimental results. Delorme et al (2009) simulated 2D sloshing and discussed the influence of viscosity and of density re-initialization on the SPH results, good agreements were obtained in terms of free surface shape and global dynamics of the flow between experimental and SPH results. Khayyer and Gotoh (2011) simulated 2D violent sloshing based on improved MPS method, obtaining impact pressure

Foundation item: Supported by National Natural Science Foundation of China (Grant Nos. 51379125, 51490675, 11432009, 51411130131)
***Corresponding author Email:** dcwan@sjtu.edu.cn

with small oscillation as well. Zhang and Wan (2012) computed liquid sloshing in 2D low-filling tank based on modified MPS method, in which good agreement between numerical results and experimental data is obtained.

Considering the complexity of the ship motion, it's essential to model liquid sloshing under six DOF motion. However, fewer 3D sloshing cases under multiple DOF excitations are computed by the self-developed meshfree particle method solver MLParticle-SJTU. In the present study, liquid sloshing in a 3D tank under sway and rolling excitations are simulated respectively to validate MLParticle-SJTU. Then, sloshing under multiple DOF excitations are simulated. The evolution of sloshing waves and impact pressure are analyzed to investigate the coupling effect of DOF.

2 Numerical Scheme

2.1 Governing Equations

In the MPS method, governing equations are the mass and momentum conservation equations. They can read as:

$$\frac{1}{\rho}\frac{D\rho}{Dt} = -\nabla \cdot \boldsymbol{V} = 0 \tag{1}$$

$$\frac{D\boldsymbol{V}}{Dt} = -\frac{1}{\rho}\nabla P + \nu\nabla \boldsymbol{V} + \boldsymbol{g} \tag{2}$$

Where ρ denotes the density, P is the pressure, V is the velocity, g is the gravity acceleration and ν the kinematics viscosity.

2.2 Particle Interaction Models

In meshfree particle method, governing equations are transformed to particle interaction equations. The interaction between particles is described through a kernel function. In this paper, we adopt the following kernel function (Zhang and Wan, 2011b):

$$W(r) = \begin{cases} \dfrac{r_e}{0.85r + 0.15r_e} - 1 & 0 \le r < r_e \\ 0 & r_e \le r \end{cases} \tag{3}$$

Where $r = |\, r_i - r_j \,|$ denotes the distance between two particles, r_e is the supported radius of the influence area of each particle. The gradient model and the divergence model is $r_e = 2.1 l_0$, while $r_e = 4.01 l_0$ is used for the Laplacian model, where l_0 is the initial distance between two adjacent particles.

To calculate the weighted average in MPS method, particle number density is defined as (Koshizuka et al., 1998):

$$< n >_i = \sum_{j \ne i} W(|\, \boldsymbol{r}_j - \boldsymbol{r}_i \,|) \tag{4}$$

This value is assumed to be proportional to the density, so the particle number density can be applied instead of density in particle discretization.

2.3 Gradient Model

In this paper, the gradient operator can be discretized into a local weighted average of radial function as follows:

$$< \nabla P >_i = \frac{D}{n^0} \sum_{j \ne i} \frac{P_j + P_i}{|\, \boldsymbol{r}_j - \boldsymbol{r}_i \,|^2} (\boldsymbol{r}_j - \boldsymbol{r}_i) \cdot W(|\, \boldsymbol{r}_j - \boldsymbol{r}_i \,|) \tag{5}$$

Where D is the number of space dimension, r represents coordinate vector of fluid particle, $W(r)$ is the kernel function and n^0 denotes the initial particle number density for incompressible flow. Eq.5 can not only improve the stability of the calculations but also maintain the momentum conservation.

2.4 Laplacian Model

Laplacian operator is derived by Koshizuka et al. (1998) from the physical concept of diffusion as:

$$< \nabla^2 \phi >_i = \frac{2D}{n^0 \lambda} \sum_{j \ne i} (\phi_j - \phi_i) \cdot W(|\, \boldsymbol{r}_j - \boldsymbol{r}_i \,|) \tag{6}$$

The parameter λ is introduced as:

$$\lambda = \frac{\sum_{j \ne i} W(|\, \boldsymbol{r}_j - \boldsymbol{r}_i \,|) \cdot |\, \boldsymbol{r}_j - \boldsymbol{r}_i \,|^2}{\sum_{j \ne i} W(|\, \boldsymbol{r}_j - \boldsymbol{r}_i \,|)} \tag{7}$$

In Eq.6, the parameter λ is introduced to keep the increase of variance equal to that of the analytical solution.

2.5 Model of incompressibility

In traditional MPS method, the incompressible condition is represented by keeping the particle number density constant. In each time step, there are two stages: first, temporal velocity of particles is calculated based on viscous and gravitational forces, and particles are moved according to the temporal velocity; second, pressure is implicitly calculated by solving a Poisson equation, and the velocity and position of particles are updated according to the obtained pressure (Tang et al., 2014).

Here we adopt a mixed source term for PPE proposed by Tanaka and Masunaga (2010), which combines the velocity divergence and the particle number density. This improved PPE is rewritten by Lee et al. (2011) as:

$$< \nabla^2 P^{n+1} >_i = (1-\gamma)\frac{\rho}{\Delta t} \nabla \cdot V_i^* - \gamma \frac{\rho}{\Delta t^2} \frac{< n^* >_i - n^0}{n^0} \tag{8}$$

where: γ is a blending parameter to account for the relative contributions of the two terms. The range of $0.01 \le \gamma \le 0.05$ is better according to numerical experiments conducted by Lee et al. (2011).

2.5 Free Surface boundary condition

In MPS, the free surface boundary conditions, including kinematic and dynamic boundary condition, are imposed. The kinematic condition is directly satisfied in Lagrangian particle method, while the dynamic condition is implemented by setting zero pressure on the free surface particles. The zero pressure condition is introduced into the solution of Poisson equation as boundary value condition, so the accuracy of surface particle detection has significant effect on pressure field.

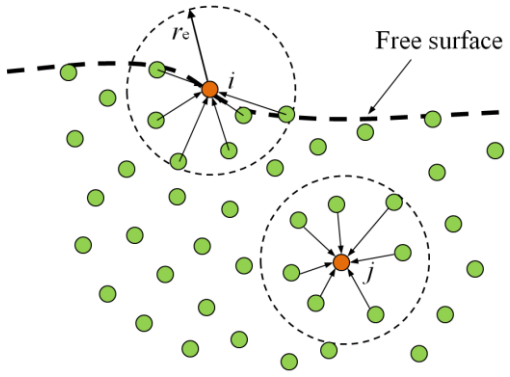

Fig.1 Description of particle interaction domain

The interaction domain is truncated in the free surface (Fig. 1), so the particle number density near the free surface is lower than that in the inner field. In traditional MPS method, particle satisfying (Koshizuka et al., 1998):

$$< n >_i^* < \beta \cdot n^0 \tag{9}$$

is considered as on the free surface, where is a parameter, can be chosen between 0.80 and 0.99.
However, inner particles with small particle number density may be misjudged as free surface particles, thus unreal pressure around the misjudged particles occur. This usually causes nonphysical pressure oscillation. To improve the accuracy of surface particle detection, we employ a new detection method in which a vector function is defined as follow (Zhang and Wan, 2011c):

$$< \boldsymbol{F} >_i = \frac{D}{n^0} \sum_{j \neq i} \frac{1}{|\boldsymbol{r}_i - \boldsymbol{r}_j|} (\boldsymbol{r}_i - \boldsymbol{r}_j) W(\boldsymbol{r}_{ij}) \tag{10}$$

The vector function $\boldsymbol{F}$ represents the asymmetry of arrangements of neighbor particles. It points out of fluid region and has a large amplitude at the free surface, but equals to zero for particles with symmetrical neighbor particles.

Thus, particles satisfying:

$$< | \boldsymbol{F} | >_i \; > \; \alpha \tag{11}$$

are considered as surface particle, where α is a parameter with a value of $0.9|F|^0$ in this paper, $|F|^0$ is the initial value of $|F|$ for surface particle.

It should be noted that the Eq. 11 is not valid for splashed particle which has no or few neighbor particles, so it is only used for particles with number density between $0.8n^0$ and $0.97n^0$. Particles with number density lower than $0.8n^0$ is definitely surface particles, while those with number density higher than $0.97n^0$ should get pressure through Poisson equation.

3 Numerical Simulations

3.1 Model validation

In this section, liquid sloshing in a 3D rectangular tank subjected to horizontal and angular motions are simulated respectively. The numerical flow patterns and impact pressure on the wall are compared with the experimental results to validate solver MLParticle-SJTU.

3.1.1 Sloshing under horizontal excitation

The first validation case is sloshing under horizontal motion, which is the same as the experimental model given by Kang and lee (2005). As shown in Fig.2, The length of the tank is L=0.8m, its height is H=0.5m, and its width is W=0.35m. The depth of water is d=0.25 m, corresponding filling level is 50%. Sloshing pressure at point P is measured. Point P is located on the left wall of the tank, 0.0575m from the bottom of the tank.

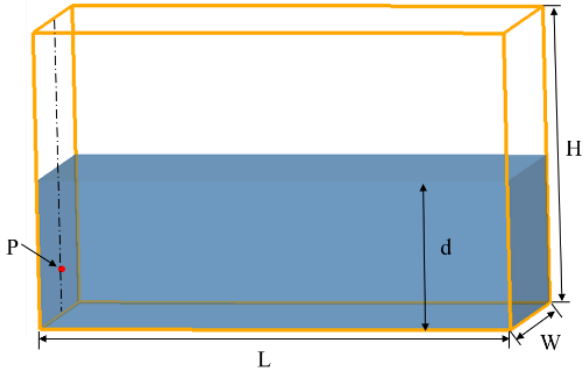

Fig.2 Schematic of the tank in the first case

The tank is subject to sinusoidal horizontal excitation:

$$x = A_x \sin(\omega t) \tag{12}$$

Where A_x is the amplitude of excitation with the value of 0.0575m, ω is excitation frequency, here ω=4.49rad/s, which is equal to the first order resonant frequency of fluid motion.

In this simulation, 750793 particles are used, among which 537579 are fluid particles. The initial particle space is 0.005 m and the time step is $5\times10^{-4}s$. The acceleration of gravity is $g=9.81m/s^2$. The density of water is $\rho=1000kg/m^3$.

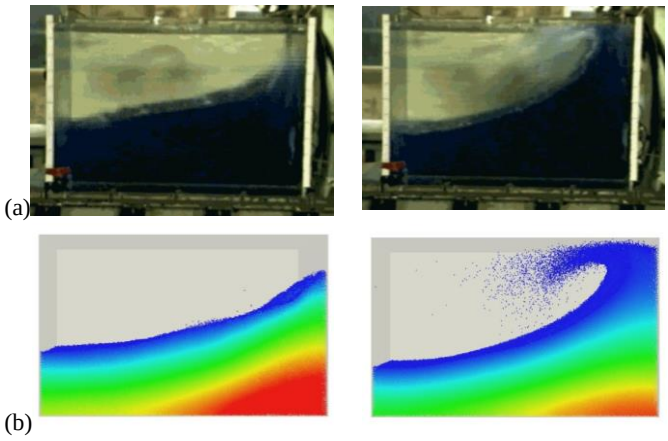

(a) Experimental results
(b) Numerical results

Fig.3 Comparison of free-surface profiles between experiment and numerical simulation

Fig.3 compares some snapshots of free surface deformation between experiment and numerical simulation. An acceptable agreement can be obtained between numerical simulation and experimental results in terms of free surface shape, such as the up-shooting phenomenon, overturned free surface and splashing water, can be capsized by MLParticle-SJTU effectively.

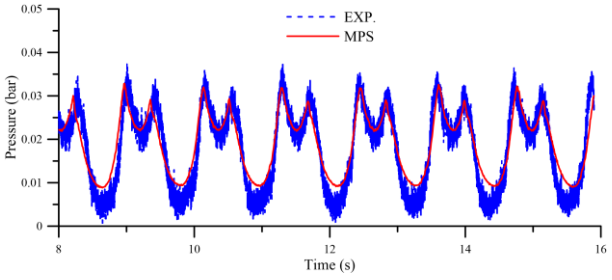

Fig.4 Comparison of impact pressure at point P between experiment and MPS method

The time history of experimental and computed pressure at point P are shown in Fig. 4. As can be seen, the global shape of the pressure curve is well reproduced by MLParticle-SJTU, which indicates that MLParticle-SJTU can predict the impact pressure induced by liquid sloshing.

From the pressure history, we can also observe that the pressure pattern looks like a typical ‘‘church roof’’ profile. When the tank reaches its maximum position on the right, the momentum direction of the fluid suffers instantaneous change. As a result, the breaking wave impinges the side wall, causing an impulsive pressure with a high peak value at point P. Then, the sloshing flow turns upward along the right-side tank wall, resulting relatively uniform pressure. Subsequently, the elevated sloshing liquid starts to break and falls from the top wall due to gravity, causing the second impact on the water lower which induces another peak value. After that the water moves toward the left-side wall, lowering the water depth near the right-side wall to below point P so the pressure is essentially zero.

3.1.2 Sloshing under angular excitation

The second validation case is sloshing excited by angular motion. The dimensions of the tank can be found in Fig.5 (Delorme L. & Souto Iglesias A, 2007). The length of the tank is L=0.9m, its height is H=0.508m, and its width is W=0.62m. The depth of water is d=0.093 m, corresponding filling level is 18.3%. Sloshing pressure at point P is measured in the simulation. Point P is located on the left wall of the tank, 0.0525m from the bottom of the tank. The rolling axis O is 0.184m over the bottom line of the tank.

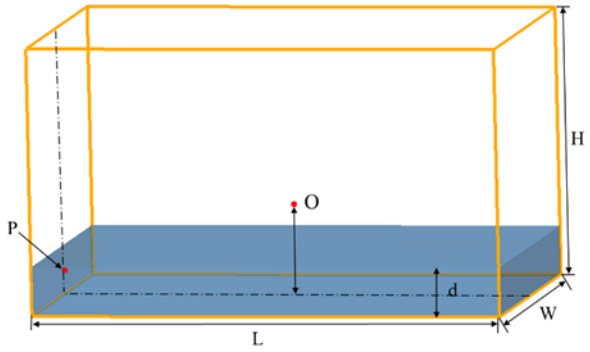

Fig.5 Schematic of tank geometry and the sensor location

The tank motion is pure rolling which follows the sinusoidal function given by:

$$\theta=\theta_0\sin(\omega_r t) \tag{13}$$

where: θ_0 is the angular displacement and ω_r is the circular frequency of rolling motion, here θ_0=4° and $\omega_r=3.29$ rad/s .

To model this problem, 726112 particles are used. Corresponding particle space is 0.005 m. The value of other parameters, such as the time step, the acceleration of gravity, the density of water and so on, is the same as the first case.

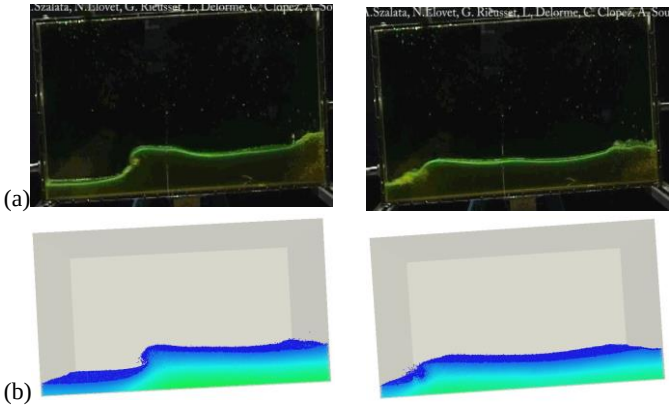

(a) Experimental results
(b) Numerical results

Fig.6 Comparison of the flow patterns between experiment and numerical simulation

The flow fields at two different moments are compared between experiment and numerical simulation in Fig.6. It can be seen that, the numerical simulation agrees with experimental results quite well, showing a good qualitative capturing of sloshing impact phenomena and of overturning waves.

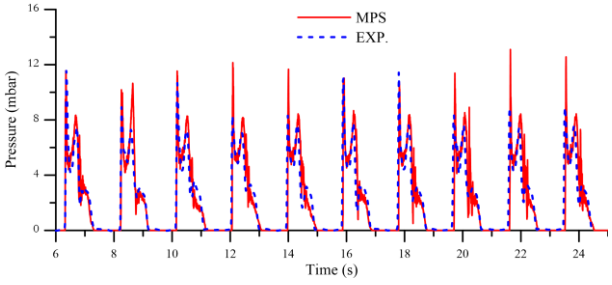

Fig.7 Comparison of impact pressure at point P between experiment and MPS method

The pressure evolution obtained by experiment and MPS method is depicted in Fig. 7. Qualitatively period can be observed in the pressure curve. Furthermore, there are two successive peaks in each period which means that in this stage, the water movement cannot catch up with the tank's rolling. When the tank has reached the maximum rolling angle and is moving back toward horizontal position, the later wave reaches the side wall of the tank and produces a second impact, showing double peaks in the pressure curve. It is found that the numerical results are in good agreement with experimental pressure value, no matter in period or amplitude, validating the present MPS method.

3.2 Sloshing under multiple DOF of motion

In this section, four 3-D liquid sloshing cases in a confined tank with multiple DOF of motion are investigated. The tank dimension and pressure probe is the same as that in Sections 3.1.1. The excitation frequency of all degrees of freedom are set to be ω=4.49rad/s, which is near the natural frequency of the water along x axis in the tank.

The translating motions of excitation are:

Surge: $x = A_x \sin(\omega t)$

Sway: $y = A_y \sin(\omega t)$

Heave: $z = A_z \sin(\omega t)$

The rotating motions of excitation are:

Roll: $\theta_x = \theta_1 \sin(\omega t)$

Pitch: $\theta_y = \theta_2 \sin(\omega t)$

Yaw: $\theta_z = \theta_3 \sin(\omega t)$

Table 1 shows the motion parameters for these four sloshing cases. As can be seen, the motion of Case A, Case B, Case C, Case D is surge, coupling of surge and pitch, coupling of surge and rolling, coupling of six DOF respectively.

Table 1 Cases for three-dimensional sloshing

	A_x (m)	A_y (m)	A_z (m)	θ_x (°)	θ_y (°)	θ_z (°)
Case A	0.02	0	0	0	0	0
Case B	0.02	0	0	0	4	0
Case C	0.02	0	0	4	0	0
Case D	0.02	0.02	0.005	4	4	2

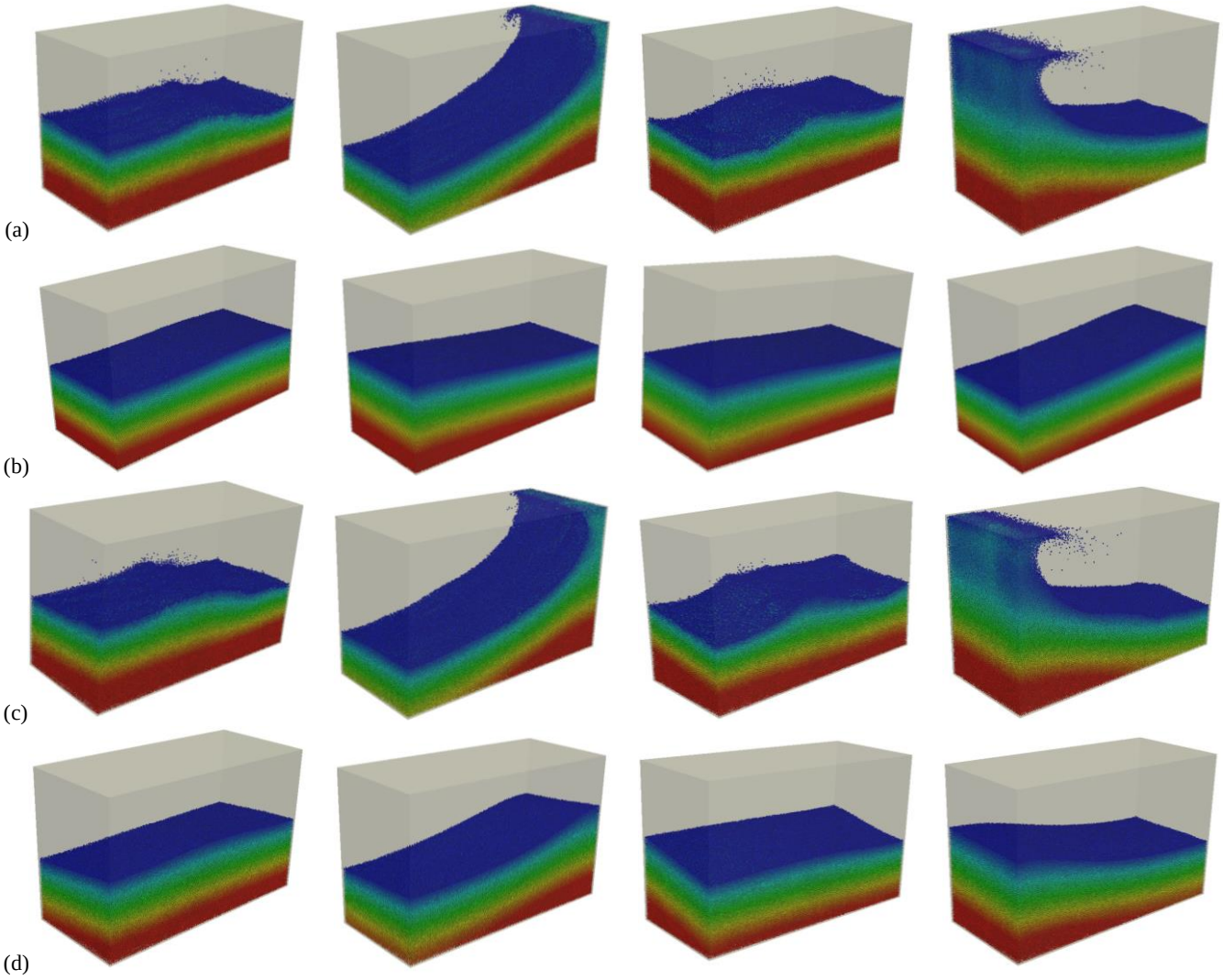

(a) Case A
(b) Case B
(c) Case C
(d) Case D

Fig.8 Evolution of the sloshing waves for different sloshing cases

Flow patterns of liquid sloshing in one period for these cases are shown in Fig.8. Fig.8 (a) shows the wave profile for only surge motion. It can be seen that flow is quite violent, with wave propagating in the tank and impacting on the side walls and ceiling of the tank. Breaking wave and splash water can be observed. When the tank reaches its maximum displacement and starts to return, liquid with large horizontal velocity impacts on the side wall and causes large impact pressure. Then an up-shooting jet is formed, which hits on the top of the tank, resulting in large impact pressure on the upper corner. After that, the jet breaks and falls down due to gravity. The falling liquid hits on the underlying liquid, and disturbs the free surface. Though the flow is violent, the present MPS is capable of computing such complicated flows.

For Case B, whose excitation is the coupling motion of surge and pitch, liquid sloshing becomes much weaker owing to the offsetting effect of the two motions. When the tank moves to right horizontally, liquid propagates to right along the motion of the tan. Meanwhile, left acceleration of the fluid owing to the left rotation of the tank may result in speed decreasing. When the amplitude of the rolling motion is large enough, the fluid will flow in the opposite. As a result, the kinetic energy of the fluid experience sharp declines. The free surface behavior becomes stable and the inertial forces are not enough to propel the liquid along the side wall to reach the top wall of the tank.

In Case C, the tank undergoes surge and rolling motion. Just as Case A, the liquid flow is also very violent. However, except for liquid motion alongside x axis, the liquid also

flows along y axis due to rolling motion of the liquid tank.

Case D is the coupling of six DOF motion. As can be seen, the free surface in Case D is much smoother than Case A. This may be due to weakening effect of these motions in different degrees of freedom.

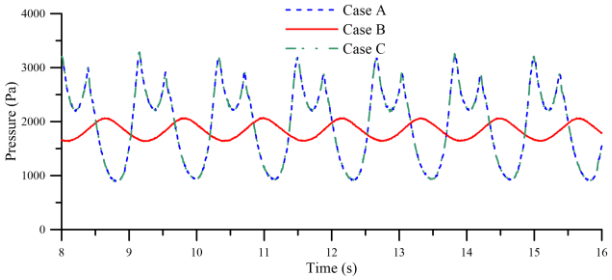

Fig.9 Comparison of impact pressure at point P between Case A and Case B

Fig.9 shows the impact pressure between Case A, Case B and Case C. It can be seen that pressure of Case B is much smaller, with the amplitude about 20 percent of the amplitude of Case A. In addition, phase difference between the two pressure curves can be observed due to different flow directions between these two cases. This is because the pitch motion is large enough to change flow direction in Case B. There is no difference between Case A and Case C, which means that rolling motion have weak effect with surge motion.

5 Conclusions

In this study, liquid sloshing in a 3D rectangular tank subjected to different DOF motion is simulated by the in house solver MLParticle-SJTU. The present numerical results agree with laboratory data.

Firstly, liquid sloshing under horizontal and angular motion is carried out to validate the present particle solver MLParticle-SJTU respectively. The comparison between the numerical flow pattern and impact pressure and the corresponding experimental data shows that MLParticle-SJTU is reliable and efficient to solve 3D sloshing problem.

Finally, four sloshing cases with motions that exhibit multiple degrees of freedom are modeled and investigated. The evolution of sloshing waves and impact pressure are analyzed to study the coupling effect of different DOF excitations. Results show that surge motion and rolling motion have weak interaction with each other. Sloshing can be damped if the amplitude and phase difference between surge motion and pitch motion are appropriate. Liquid sloshing under six DOF excitations can be modelled by MLParticle-SJTU.

Acknowledgement

This work is supported by National Natural Science Foundation of China (Grant Nos. 51379125, 51490675, 11432009, 51411130131), The National Key Basic Research Development Plan (973 Plan) Project of China (Grant No. 2013CB036103), High Technology of Marine Research Project of The Ministry of Industry and Information Technology of China, Chang Jiang Scholars Program (Grant No. T2014099) and the Program for Professor of Special Appointment (Eastern Scholar) at Shanghai Institutions of Higher Learning (Grant No. 2013022), to which the authors are most grateful.

References

Cui Y, LIU H (2009). Numerical simulation of sloshing in two dimensional rectangular tanks with SPH. JSCE Annual Journal of Hydraulic Engineering, 53, 181-186.

Delorme L, Souto-Iglesias A (2007). Impact pressure test case description, ETSIN Report.

Delorme L, Colagrossi A, Souto-Iglesias A (2009). A set of canonical problems in sloshing, Part I: Pressure field in forced roll—comparison between experimental results and SPH. Ocean Engineering, 36(2), 168-178.

Gingold RA, Monaghan JJ (1977). Smoothed particle hydrodynamics-Theory and application to non-spherical stars. Royal Astronomical Society, 181, 375-389.

Hu CH, Kashiwagi M, Kishev Z (2004). Numerical simulation of violent sloshing by CIP method. IWWWFB International Workshop Water Waves Floating Bodies, Cortona.

Kang DH, Lee YB (2005). Summary report of sloshing model test for rectangular model. Daewoo Ship building & Marine Engineering Co., Ltd., South Korea.

Kim Y (2001). Numerical simulation of sloshing flows with impact load. Applied Ocean Research, 23 (1), 53-62.

Koshizuka S, Oka Y (1996). Moving Particle Semi-implicit method for fragmentation of incompressible fluid. Nuclear science and engineering, 123(3), 421-434.

Koshizuka S, Obe A, Oka Y (1998). Numerical analysis of breaking waves using the Moving Particle Semi-implicit method. International Journal for Numerical Methods in Fluids, 26(7): 751-769.

Khayyer A, Gotoh H (2011). Enhancement of stability and accuracy of the Moving Particle Semi-implicit method. Journal of Computational Physics, 230(8), 3093-3118.

Lee BH, Park JC, Kim MH, Hwang SC (2011). Step-by-step improvement of MPS method in simulating violent free-surface motions and impact-loads. Computer methods in applied mechanics and engineering, 200(9), 1113-1125.

Liu DM, Lin PZ (2008). A numerical study of three-dimensional liquid sloshing in tanks. Journal of Computational Physics, 227(8), 3921-3939.

Shao JR, Li HQ, Liu GR, Liu MB (2012). An improved SPH method for modeling liquid sloshing dynamics. Computers and Structures, 100, 18-26.

Tanaka M, Masunaga T (2010). Stabilization and smoothing of pressure in MPS method by Quasi-Compressibility. Journal of Computational Physics, 229, 4279-4290.

Tang ZY, Zhang YX, Wan DC (2014). Overlapping MPS Method for 2D Free Surface Flow. ISOPE International Society of Offshore and Polar Engineers, Busan, 3, 411-419.

Wu CH, Chen BF (2009). Sloshing waves and resonance modes of fluid in a 3D tank by a time-independent finite difference method. Ocean Engineering, 36(6), 500-510.

Zhang YX, Wan, DC (2011a). Application of MPS in 3D dam breaking flows (in Chinese). Scientia Sinica Physica, Mechanica & Astronomica, 41(140), 140–154.

Zhang YX, Wan DC (2011b). Apply MPS method to simulate motion of floating body interacting with solitary wave. IWSH International Workshop on Hydrodynamics, Shanghai, 275-279.

Zhang YX, Wan DC (2011c). Application of improved MPS method in sloshing problem. Proc. of the 23rd Chinese Symposium on Hydrodynamics, Xi'an.

Zhang YX, Wan, DC (2012). Numerical simulation of liquid sloshing in low-filling tank by MPS. Chinese Journal of Hydrodynamics, 27(1), 100-107.